

# JAMES | Journal of Advances in Modeling Earth Systems



### RESEARCH ARTICLE

10.1029/2019MS001975

#### **Key Points:**

- A clustering-based genesis model is developed to better simulate tropical cyclone (TC) interannual variability
- An analog-wind track model is developed to simulate TC trajectory based on both historical patterns and surrounding wind features
- The integrated TC model is able to simulate TC climatology, including statistics of landfall frequency and intensity

#### Correspondence to:

R. Jing, jingrenzhi.go@gmail.com

#### Citation:

Jing, R., & Lin, N. (2020). An environment-dependent probabilistic tropical cyclone model. *Journal of Advances in Modeling Earth Systems*, 12, e2019MS001975. https://doi.org/10.1029/2019MS001975

Received 18 DEC 2019 Accepted 27 FEB 2020 Accepted article online 10 MAR 2020

# ©2020. The Authors. This is an open access article under the terms of the Creative Commons Attribution-NonCommercial License, which permits use, distribution and reproduction in any medium, provided the original work is properly cited and is not used for commercial purposes.

# An Environment-Dependent Probabilistic Tropical Cyclone Model

Renzhi Jing<sup>1</sup> and Ning Lin<sup>1</sup>

<sup>1</sup>Department of Civil and Environmental Engineering, Princeton University, Princeton, NJ, USA

**Abstract** The Princeton environment-dependent probabilistic tropical cyclone (PepC) model is developed for generating synthetic tropical cyclones (TCs) to support TC risk assessment. PepC consists of three components: a hierarchical Poisson genesis model, an analog-wind track model, and a Markov intensity model. The three model components are dependent on environmental variables that vary with the climate, including potential intensity, advection flow, vertical wind shear, relative humidity, and ocean-cooling parameters. The present model is developed for the North Atlantic Basin. The three model components and the integrated model are verified against observations using out-of-sample testing. The model can generally capture the TC climatology and reproduce statistics of TC genesis, movement, rapid intensification, and lifetime maximum intensity, as well as local landfall frequency and intensity. It can be coupled with climate models and TC hazard models to quantify TC-related wind, surge, and rainfall risks under various climate conditions. The modeling framework can be further improved when more relevant environmental variables are identified and become available in climate model outputs.

Plain Language Summary The Princeton environment-dependent probabilisitic tropical cyclone model (PepC) is developed to generate synthetic tropical cyclones (TCs). The PepC has three components: a genesis model that simulates the time and location of a storm's formation, a track model that simulates the storm's movement over the ocean, and an intensity model that simulates the storm's maximum wind speed evolving along the track. We evaluate PepC's performance by comparing simulated TCs with historical records in the North Atlantic Basin. Our results show that under the current climate, simulated TCs from PepC match well with observations in many aspects, including wide TC counts and local landfall intensity. As all of its three model components are dependent on environmental variables that vary with the climate, PepC is able to generate synthetic storms under various climate conditions. The synthetic TCs generated from PepC can be applied to quantify TC-related wind, surge, and rainfall risks in a changing climate.

#### 1. Introduction

Tropical cyclones (TCs) are among the most deadly and destructive natural phenomena in the world. Accounting for 17% of the total number of billion-dollar weather and climate disasters, TC caused more than 50% of the total damages, according to Smith and Matthews (2015) in a study of U.S. climate disasters in 1980–2013. Continuously improving our understanding of TC-related hazards and risk under current and future climates is of great importance.

There are two general approaches to assess TC hazards (i.e., extreme winds, heavy rainfall, and storm surges) and risk. Local models estimate TC hazards at a specific location of interest based on historical TCs that affected the region or larger synthetic TC datasets generated based on those historical TCs (Irish & Resio, 2013; Jagger et al., 2001; Mumane et al., 2000; Tolwinski-Ward, 2015). These site-specific models perform relatively well in regions with high TC activity but are not accurate when historical data are limited (Hall & Jewson, 2008). To overcome the data limitation at the local scale, basin-wide models make use of all historical storms in the ocean basin to generate synthetic TCs from genesis to lysis over the entire basin (Vickery et al., 2000). Specifically, a basin-wide model may include three components: a genesis model that simulates the temporal and spatial variation of TC formation, a track model that propagates the generated storms, and an intensity model that estimates the intensity evolution along the storm track. The storm is considered dissipated if its intensity is lower than a given threshold.

JING AND LIN 1 of 18



Ideally, the generated synthetic TCs are fully dependent on the storm environment so that they vary consistently with the change of the climate conditions. However, most synthetic TC models currently in use are largely climate invariant. James and Mason (2005) generate storms based mostly on historical storm properties. Hall and Jewson (2007) simulate storm tracks using near-neighbor historical information. Vickery et al. (2000, 2009) simulate storms using mainly storm predictors plus limited environmental variables such as sea surface temperature (SST), and the model coefficients depend on (historical) storm locations. These models are not suitable for risk assessment under a changing climate. More recent models have started to include environmental dependence by adding large-scale environmental predictors, such as El Nino-Southern Oscillation (ENSO) indices. The genesis and track components of the model developed by Yonekura and Hall (2011) are dependent on ENSO indices. Though such a model can better capture the effect of ENSO state on TC seasonality, the large-scale indices have limited capability in reproducing local variations. Yonekura and Hall (2014) improved their genesis component by introducing local SST as an environmental predictor.

The statistical-deterministic model developed by Emanuel et al. (2008) has become a principle method that can generate large numbers of synthetic TCs at the basin scale driven by comprehensive local climate conditions. The model applies a random seeding method to initiate the storm, a beta and advection model (BAM) based on local winds to propagate the storm, and a deterministic Coupled Hurricane Intensity Prediction System (CHIPS; Emanuel et al., 2004) model to estimate the storm intensity based on local thermodynamic state of the atmosphere and ocean. The model has been widely applied to assess TC wind (Yeo et al., 2014), rainfall (Emanuel, 2017), and storm surge (Marsooli et al., 2019) hazards and TC economic losses (Mendelsohn et al., 2012), under current and future projected climate conditions. More recently, Lee et al. (2018) developed a synthetic TC model that also depends on the local environment but is based purely on statistical modeling. In this model, the genesis formation is simulated on regular grids over the ocean basin based on a Poisson regression on the TC genesis index (TCGI; dependent on absolute vorticity, relative humidity, relative SST, vertical wind shear, and storm location) developed by Tippett et al. (2011), the storm is propagated based on a revised BAM with the beta drift dependent on the storm location, and the storm intensity is estimated based on a multiple linear regression on environmental (potential intensity, wind shear, relative humidity) and storm (current intensity, previous-step intensity change, and translation speed) variables plus a stochastic error term (Lee et al., 2015, 2016a).

Following Emanuel et al. (2008) and Lee et al. (2018), we develop a new climate-dependent probabilistic TC model. The new model is called PepC, short for Princeton environment-dependent probabilistic tropical cyclone model. PepC consists of three components: a hierarchical Poisson genesis model, an analog-wind track model, and a Markov intensity model. The genesis model is developed based on a Poisson regression on four environmental variables: the potential intensity, relative humidity, wind shear, and absolute vorticity. Unlike Lee et al. (2018), the Poisson regression and genesis simulation are performed on clustering grids (formed based on the variation of the environmental variables), to avoid the zero-inflation problem associated with regressing sparse genesis data on a regular grid. The analog-wind track model determines the storm track based on local in situ wind as well as historical track patterns, to overcome the regression challenge induced by the naturally large variations and uncertainties of local winds. The intensity component developed in our previous work, the Markov environment-dependent hurricane intensity model (MeHiM; Jing & Lin, 2019), lets the storm evolve among different states (i.e., slow, moderate, and rapid) of intensity change as a response to the change of environmental variables (potential intensity, relative humidity, wind shear, and an ocean feedback parameter), lifting the basic assumption of a linear model that the response of intensity change to the environmental change is homogenous. These changes/improvements of the model components over previous methods may help better capture TC frequency and interannual variability, track patterns and variations, and intensity extremes associated with rapid intensification, supporting improved TC hazard and risk analysis.

To verify the performance of PepC, we first evaluate each model component and then the integrated modeling system, by comparing observed and simulated TC climatology over the North Atlantic (NA) basin. As the genesis model simulates local counts based on local environmental parameters, we examine whether the model can reproduce basin-wide interannual, seasonal, and spatial distributions of observed genesis. Also, we evaluate if the track model can reproduce observed distribution of track density over the basin and landfall frequency along the Mexico and U.S. East and Gulf coastlines. Then, we couple the intensity component

JING AND LIN 2 of 18



(MeHiM, evaluated in Jing & Lin, 2019) with the genesis and track components and investigate if the integrated TC model PepC can capture the statistics of rapid intensification, lifetime maximum intensity, and landfall frequency and intensity.

This paper is organized as follows. Following this introduction, section 2 describes the data used in this work. section 3 describes the development of the genesis and track components and briefly introduces the recently developed TC intensity model. section 4 describes the integrated TC model PepC. section 5 provides discussions, and section 6 summarizes the main findings of the study.

#### 2. Data

The genesis and intensity components are developed based on historical records from 1979 to 2014 in the NA basin, while the track component is developed based on historical records from 1979 to 2014 as well as 1948 to 1979 (to generate analog track information). The TC dataset is taken from the IBTrACS WMO archive (Knapp et al., 2010). It includes for each storm 6-hourly latitude and longitude positions and 10-minute maximum sustained wind speeds at 10 m above the sea surface, which are used to calculate the storm's current intensity change (DV), previous-step intensity change (DVp), and current intensity (V).

The atmospheric variables are derived from the ERA-Interim Reanalysis with a resolution of  $0.75^{\circ} \times 0.75^{\circ}$  produced by the European Centre for Medium-Range Weather Forecasts (ECMWF; Dee et al., 2011). Storm's potential intensity, PI, is theoretically derived following Emanuel (1995, 1988) and Bister and Emanuel (1998, 2002). The mid-level relative humidity, RH, is computed as the averaged relative humidity in the layer between 500 and 700 hPa within the 500- to 800-km annulus around the storm center. The low-level relative vorticity is defined as the vorticity at 850 hPa, averaged over the 200- to 800-km annulus around the storm center. The absolute vorticity, VO, is computed as the sum of relative vorticity and the vorticity of the earth. The deep layer vertical wind shear, SHR, is defined as the difference between the 850- and 200-hPa level winds, averaged over the 200- to 800-km annulus around the storm center. The 850- and 250-hPa level winds used in the track model are also averaged over the 200- to 800-km annulus around the storm center. In addition to atmospheric variables, an ocean feedback parameter (OCN), developed by Schade and Emanuel (1999) based on numerical modeling, is used to represent the ocean's negative impact on storm intensification. The OCN is dependent on storm's translation speed, ocean mixed later depth, and thermal stratification below the ocean mixed layer. The ocean's salinity and potential temperature are taken from the Ocean Reanalysis System 4 (ORAS4; Balmaseda et al., 2013).

In this work, the genesis component is developed to predict TC formation based on PI, SHR, VO, and RH. The track component is developed to predict TC movement based on local winds and analog predictors formed by historical track patterns. In MeHiM, DV is estimated based on six variables: DVp, V, PI, SHR, RH, and OCN.

# 3. Model Components

#### 3.1. Genesis

The genesis model component determines how many storms form in a year and where they originate over the ocean basin. Previous genesis models may be roughly classified into two categories. In the first category, the genesis rate and origination rely little on environmental variables. Hall and Jewson (2007) determines the TC annual rate by sampling from a Poisson distribution based on historical records. Vickery et al. (2000, 2009) simulate the annual rate similarly but from a fitted negative binomial distribution. In both models, the starting position and time of the storms are directly sampled from the historical data. The genesis component of the statistical-deterministic model of Emanuel et al. (2008) initiates storms by random seeding, assuming a uniform distribution of storm formation. The initiated storms are then selected by the track and intensity models, and the annual rate is calibrated with the observation.

The second category includes multiple TC genesis indices based on large-scale environmental parameters. Gray's TC genesis theory (Gray, 1975) showed that the temporal and spatial variability of genesis is related to a limited number of large-scale environmental predictors, among which the low-level relative vorticity, vertical wind shear, ocean thermal energy, and mid-level humidity are of great importance. Based on these findings, Emanuel and Nolan (2004) introduced a genesis index, the genesis potential index (GPI), which is

JING AND LIN 3 of 18



an empirical function of PI, SHR, VO, and RH. They further proposed a revised GPI, which is dependent on entropy deficit (Emanuel et al., 2008) other than RH, based on theoretical and modeling considerations (Emanuel, 2010). Tippett et al. (2011) developed the TCGI describing the annual expected storm number as the exponential of a linear combination of SHR, VO, RH, relative SST, and a location term. Menkes et al. (2011) showed that, compared with Gray's genesis index and GPI, TCGI has less bias and a better fit to the observations at the seasonal scale. The TCGI can be directly applied as the mean of an assumed (nonhomogenous) Poisson process of storm formation, which Lee et al. (2018) have adopted to simulate synthetic TC genesis.

Although dependent on environmental variables and applicable for climate change studies, TCGI, as well as other TC genesis indices, has limitations in simulating the accurate number of storms on both seasonal and interannual scales. According to a recent study comparing the TC genesis indices, all indices tend to overestimate cyclogenesis during unfavorable seasons and strikingly underestimate the amplitude of interannual variability (Menkes et al., 2011). Also, almost all indices tend to have an equatorward bias in predicting the cyclogenesis areas, though this error can be greatly reduced by using a "clipped" vorticity in TCGI (Menkes et al., 2011). Considering these limitations, we build a new climate-dependent TC genesis model particularly focusing on the model's ability to capture the temporal and spatial variations of storm genesis.

#### 3.1.1. Model Developments

Similar to Tippett et al. (2011) and Lee et al. (2018), we apply a Poisson framework to model TC genesis on a local grid scale (rather than on the basin scale). The Poisson framework assumes that the forming TCs are conditionally independent (given the climate environment), and one storm would not affect the other. Though special cases exist when storms appear to be close together at the same time or even collide, these events are rare and not well understood (Schenkel, 2016). Given Poisson-distributed TC genesis, the annual count of storms over the basin is theoretically Poisson distributed, which was shown to be approximately consistent with observational data (Rumpf et al., 2007, 2009). In addition, TC landfall theoretically follows a Poisson process, which is also consistent with observations (Lin et al., 2012). Under the Poisson framework, the expected number of TC genesis events is log-linearly dependent on the climate variables:

$$\log(\text{TCGR}) = b + b_{\text{VO}}\text{VO} + b_{\text{SHR}}\text{SHR} + b_{\text{RH}}\text{RH} + b_{\text{PI}}\text{PI}, \tag{1}$$

where TC genesis rate (TCGR) represents the expected number of storms in a grid cell. VO, SHR, RH, and PI are grid-averaged monthly mean absolute vorticity at 850 hPa, vertical wind shear between the 850 and 200 hPa levels, relative humidity at 600 hPa, and potential intensity, respectively. Unlike Tippett et al. (2011) and Lee et al. (2018) using relative SST, we select the more comprehensive PI as the thermodynamical variable, which is also consistent with the intensity component of PepC. Also, we remove the location term used by Tippett et al. (2011) and Lee et al. (2018), so that the model contains only physical climate variables and does not depend on historical genesis locations. We select RH to represent the dependence on water vapor, and we discuss the effect of the variable selection between RH and another humidity variable, the entropy deficit, in Section 4.

A more significant difference from the TCGI model in Tippett et al. (2011) and Lee et al. (2018) is that instead of using regular grids, we fit the Poisson regression model based on clustering grids that contain similar environmental fields. Given the sparsity of the genesis data, applying the Poisson regression model on regular grids has challenges. Applying a relatively large grid size will smooth out variations and underestimate extremes, while applying a relatively small grid size will induce excess zeroes, leading to the zero-inflation problem. In either situation, the magnitude of spatial and temporal variations will be reduced. On the other hand, clustering grids can be subjectively set to avoid this dilemma, helping to reconcile the spatial continuity of the environment fields and discreteness of storm occurrences.

Specifically, for each month of each year in the training dataset, first we divide the entire basin (7.5–40°N, 262.5-346°E) into regular grids at a spatial resolution of  $2.5^{\circ} \times 2.5^{\circ}$ , and then we group the regular grids into clustering grids according the similarity of the monthly grid-averaged environmental fields. To do so, we apply a graph-based clustering method proposed by Felzenszwalb and Huttenlocher (2004), rather than the traditional k-means clustering, to ensure spatial connectivity. The clustering algorithm does not require a predefined number of clusters but determines this number based purely on the variation in the environmental fields. Technically, the algorithm takes a feature affinity (homogeneity) threshold as input to

JING AND LIN 4 of 18

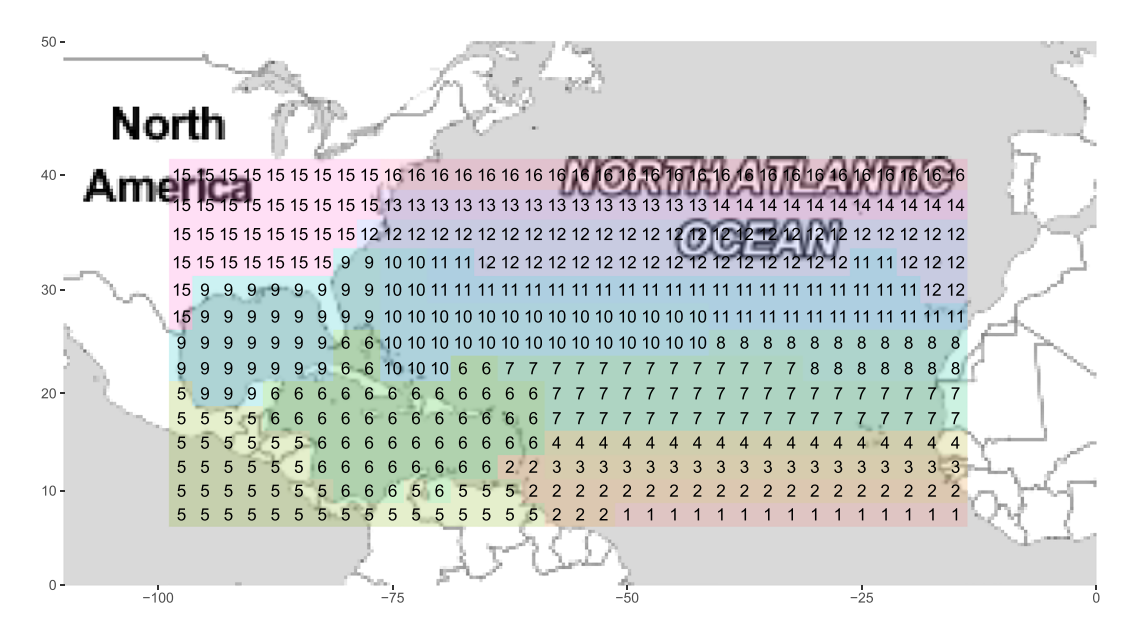


Figure 1. Example of graph-based segmentation over the NA basin for genesis modeling. The map shown is for the month of July in 1979. The entire basin is clustered into 16 connected regions. Cluster 15 and cluster 5 are excluded in the modeling since they are either over land or out of the NA basin. The environmental data is taken at a resolution of  $0.75^{\circ} \times 0.75^{\circ}$ , while the regular grid is at a resolution of  $2.5^{\circ} \times 2.5^{\circ}$ . A regular grid is considered as land if more than half of its data is over land.

determine if two neighboring grids should be merged to form a larger grid. This affinity threshold (k = 0.01), set as a constant for all months, is determined by cross validation. This single threshold directly measures the environmental homogeneity and is more subjective than setting arbitrarily the number of clusters. Before clustering, we normalized each environmental variable so that all features are numerically comparable and contribute equally to the cluster identification. As a result, for each month, the entire basin is divided into a set of connected clusters based on local environmental variables. The more homogeneous the environmental fields over the basin, the fewer clusters form in the basin, and the environmental variables are considered homogeneous within each cluster. An example of clustered grids is shown in Figure 1, in which the entire basin is divided into 16 clustered grids. After clustering, the storm counts and averaged environmental fields over all clustered grids and all months are collected to perform the Poisson regression (equation 1).

To evaluate the model, we use 27 years of historical data (1979–2005) for model development and leave the remaining 9 years (2006–2014) of data for out-of-sample evaluation. Environmental variables are standardized by subtracting the mean and dividing by standard deviation before fitting the model. The estimated model coefficients are shown in Table 1. As expected, PI, RH, and VO are positively correlated to cyclogenesis, while SHR is detrimental to storm formation. The negative intercept indicates that it is very unlikely to have storms generated when all environment variables are at their mean. This result also helps to explain the rareness of TCs, which happen only in favorable rather than mean-state environments.

#### 3.1.2. Evaluation

The performance of the genesis model is evaluated by comparing model simulations with observations. When applying the model to new data (e.g., new monthly environmental variables in 2006–2014 for model testing), we need to divide the basin into connected clusters. More specifically, to simulate the storms in a specific month, we first use the graph-based segmentation algorithm to divide the basin into clusters according to the similarity among local environmental variables for the month. Then, we compute the cluster-averaged environmental variables and then apply equation 1 to obtain the monthly Poisson rate for each cluster. Given the count, randomly drawn from the obtained Poisson distribution, the genesis location is drawn uniformly within the cluster and a formation date is selected uniformly during the month, to be consistent with the Poisson theory. Repeating the above processes, we simulate TC genesis climatology in the period of 1979–2014 by constructing 100 independent 36-year realizations.

JING AND LIN 5 of 18



Table 1           Coefficients of the clustering-based genesis model							
Intercept	PI	RH	VO	SHR			
-4.084	1.334	0.725	0.942	-0.816			

The time series of annual rates of observed and simulated storms over the basin are shown in Figure 2. There are on average 15.51 storms per year generated in the simulation, very close to the historical observation of 15.41 storms per year, over the period of 1979–2014. The correlation coefficient between the observed and simulated (median of the 100 realizations) annual count is relatively high (0.74 on training

set and 0.72 on testing set). The genesis model can capture the interannual variation under different ENSO phases, simulating more storms in strong La Nina years (e.g., 1988 and 2010) than in strong El Nino years (e.g., 1982 and 1997). The modeled magnitude of interannual fluctuations is about 14 TCs (the median), smaller than that of 26 TCs in the observation. However, this clustering-based genesis model outperforms the genesis model developed based on regular grids particularly at the interannual scale, as the magnitude of interannual fluctuations is predicted as 8 TCs using regular grids (figure not shown). While the previous GPI and TCGI models were found to have limited ability to reproduce the amplitude of interannual variability (Menkes et al., 2011), our genesis model produces a standard deviation of 4.12 for the annual rate, which is very close to that of 4.33 in observation (for both training and testing datasets). For seasonal variability, as shown in Figure 3 for the monthly storm count, the simulation captures the active and nonactive seasons, although the model slightly overestimates the storm count in unfavorable seasons, especially in July, while it underestimates the storm counts from August to December. Such a relatively weak variability on the seasonal scale of the model is also seen in the GPI and TCGI models (Menkes et al., 2011).

A comparison of spatial distribution of the genesis in the observation and in one selected simulation is shown in Figure 4. The local counts are normalized by the maximum grid count over the entire basin. The simulation generally captures the observed spatial pattern and has local maxima in approximately the right locations, although it has lower peak values, especially in the main development region (10°N–20°N, 80°W–20°W). The spatial extension of the simulation is also wider than the observation, with some simulated storms occurring 40°N, which is rarely seen in the observation. The genesis model may predict a nonzero probability of storm formation in a location or month where no TC genesis events have been observed in the history. Similar to results from previous TC index models, the simulated genesis locations are also slightly shifted equatorward, probably because the influence of the Coriolis term on TC genesis is not well represented in the environmental variables (there is no explicit location term in our model).

#### 3.2. Track

Given the genesis formation, the track model determines the storm's movement and landfall location. In previous studies, the simplest track models propagate storms by resampling translation speed and changes in the direction of movement from historical TCs that are close to the storm's current position (Rumpf et al., 2007, 2009). Since storm persistence is shown to be an important predictor, several auto-

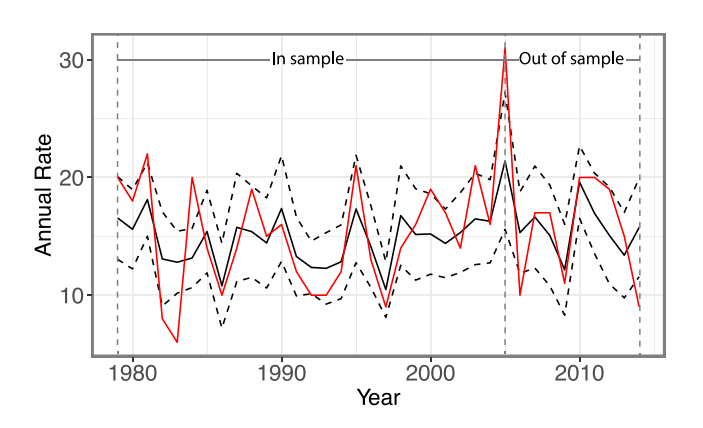


**Figure 2.** Comparison of simulated (black) and observed (red) TC annual frequency. The solid black line represents the median of 100 simulations, and dashed black lines represent the one standard deviation from the median of the 100 simulations.

regressive models and their variations have been developed by Vickery et al. (2000, 2009), James and Mason (2005), and Hall and Jewson (2007) to generate synthetic tracks. Another important category of track models based on TC predictors is hurricane analog models. Hurricane Analog (HURRAN), developed by Hope and Neumann (1970), is such an example that has been applied to operational track forecasting. In this model, historical tracks that meet the requirements of both appearing in the similar region and time of the year and having similar heading and translation speed are selected as analog tracks, to inform the displacement of the current storm. These above-mentioned models rely on historical storm tracks and may perform well under the current climate, but they are unsuitable for track simulation under a changing climate.

Emanuel et al. (2006) applied a beta-advection model (BAM; Marks, 1992) coupled with local synthetic wind, under the assumption that storms move with vertical mean advection plus the effect of beta drift. The model has been adopted by Lee et al. (2018), where they revised the constant beta

JING AND LIN 6 of 18

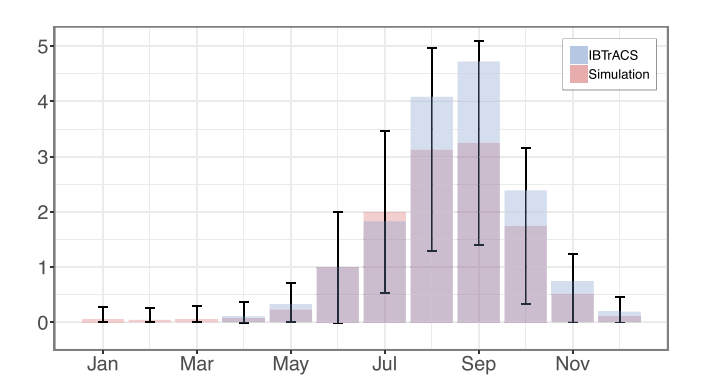


**Figure 3.** Comparison of seasonal variation of simulated (blue) and observed (red) genesis. The black error bar represents the one standard deviation range of 100 independent 36-year simulations.

drift to be location dependent. BAM works well with synthetic winds, as shown in Emanuel et al. (2006); however, a direct regression of historical track movement on observed winds does not perform well, probably due to the large temporal–spatial variation in local winds. In this work, we aim to develop a new track model that follows the steering wind assumption in BAM but overcomes the challenge of large local-wind variation by also incorporating analog track patterns.

#### 3.2.1. Model Developments

We develop our track model with predictors based on both similar historical tracks and local winds. However, in contrast to HURRAN, where similarity is defined mainly based on storm location and date in the year, we define similarity based on only the two-step (12-hr) track shape. Thus, although the model depends on historical tracks (over the entire basin), it does not depend on the storm location (as in, e.g., Vickery et al., 2009). Since TCs are driven mostly by background steering wind, the similarity

among TC tracks in return implies similar steering winds. Thus, TCs that share a similar existing trajectory would be more likely to move in a similar pattern in the next step.

We firstly develop an analog track model that depends purely on track analog predictors. Then, we incorporate in situ winds as additional environmental predictors to further improve the model. Intuitively, the analog predictors generated from past track data reflect the mean background steering winds, while the wind predictors govern the variation due to real-time in situ winds.

#### 3.2.1.1. Analog Track Model

To generate analog predictors, we first prepare a track segment pool from historical TCs to be used for similarity matching. We discretize full TC tracks into 6 hourly segments and obtain ~10,000 two-step track segments from 415 observed TCs in the period of 1948–1978. Then, for each new storm, its current location and previous two locations form a two-step query of track segments. We search similar segments in the segment pool based on the Euclidean distance between the vectors, and the best-matching track segments are selected as guidance for propagating the storm in the next step.

Specifically, we build a random forest regression model to map analog track predictors to real storm displacement. The analog track predictors are selected as the mean and standard deviation values of best-matching track segments. Each mean displacement represents a hypothetic movement and its standard deviation is a

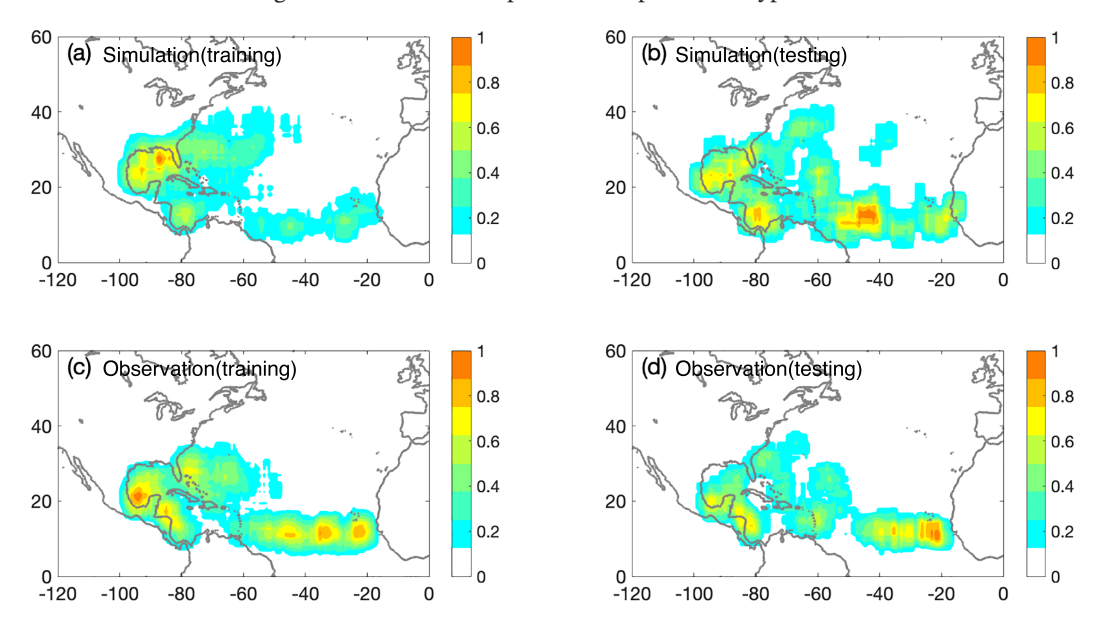


Figure 4. Comparison of spatial distribution of genesis in (a,b) simulations and (c,d) observations, in the (a,c) training dataset and (b,d) testing dataset. Genesis number is shown as the number of storms in each  $0.75^{\circ} \times 0.75^{\circ}$  grid box normalized by the highest grid count over the entire basin (so the values are in the range of 0 and 1). The data are then smoothed with a Gaussian low-pass filter.

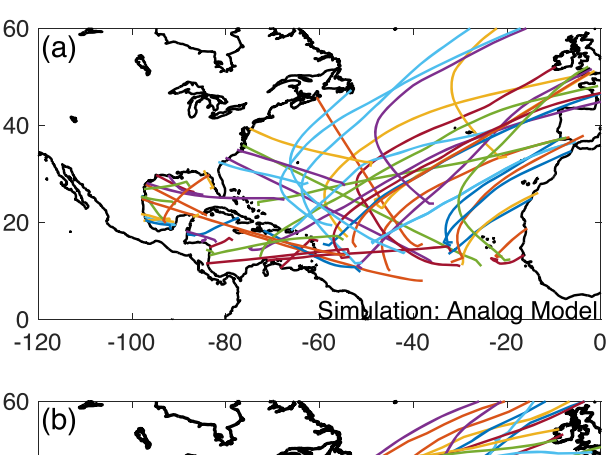
JING AND LIN 7 of 18

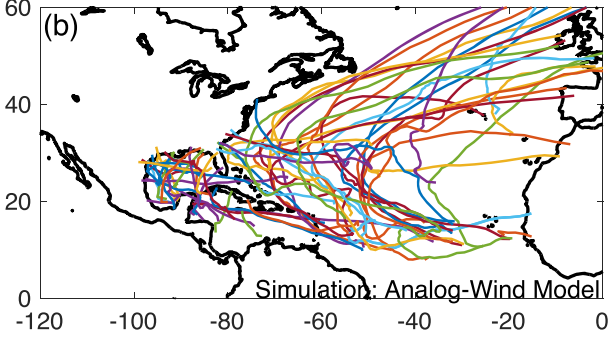


Table 2

Performance of analog track model and analog-wind track model. The numbers shown are percent of the variance explained by the model  $(R^2)$  for 6-hourly displacement in zonal and meridional directions, using training dataset and testing dataset

	Zonal	Zonal		Meridional	
	Train	Test	Train	Test	
Analog Analog-wind	0.95 0.95	0.93 0.93	0.89 0.90	0.83 0.84	





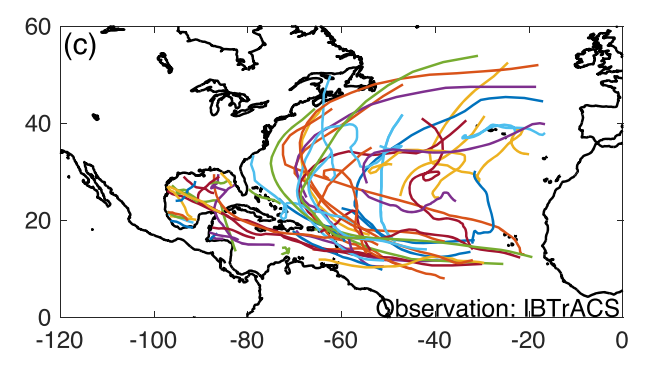


**Figure 5.** Sixty randomly selected tracks from (a) analog track model simulation, (b) analog-wind track model simulation, and (c) IBTrACS. To be consistent with the simulations, the historical tracks are terminated when they hit land.

measurement of the confidence for this hypothetic movement. For example, if the observed next step displacements from 10 best-matching track segments are close to each other, accordingly the standard deviation is small. On the other hand, if the observed next step displacements are quite random, the large standard deviation indicates a low confidence in following the mean pattern. In practice, we select a series number of best-matching track segments, from the most similar one track segment to the most similar 10% track segments, and calculate the mean and standard deviation values of the series of suggested movements as the analog predictors. A sensitivity test indicates that the model is not very sensitive to the number of selected best-matching storms, and any selections that can well represent the population of the most similar <10% tracks can be good analog predictors.

## 3.2.1.2. Analog-Wind Track Model

In the analog model, we use only analog predictors from the historical data; no direct wind data is included. To account for the impact of real-time in situ winds, we build an analog-wind model by adding meridional and zonal winds at 850 and 250 hPa (similar to Emanuel et al., 2006) as four additional dependent variables in the random forest regression model.

This analog-wind model improves over previous studies in several aspects. First, since in situ real-time winds vary the greatest in space and time among all meteorological variables, we manage to reduce this uncertainty by representing steering winds partially with analog predictors. Second, we select two-step track segments instead of longer segments to emphasize the effect of the local wind, since storms may not respond to winds earlier than 12 hour before. Lastly, through TC analogs, we manage to take movement inertia into consideration as it takes time for storms to respond to the winds.

Both the analog track model and the analog-wind model are built on 417 TCs in the period of 1979–2005 and are tested on the 138 TCs in the period of 2006–2014. The results for both training dataset and testing dataset are shown in Table 2. The  $R^2$  values are between 0.83 and 0.93 for the testing dataset. As a comparison, the  $R^2$  for the track model with only the local wind predictors is around 0.6 in both directions, and thus adding analog predictors improves track model dramatically. Similar to Emanuel et al. (2006), in both analog and analog-wind models, the prediction of the movement for the meridional direction is slightly better than that for the zonal direction. Adding in situ wind predictors only slightly increases the statistical  $R^2$ ; however, the wind components are of great importance in controlling the meandering behavior of storms over the ocean, as discussed in the next subsection.

# 3.2.2. Evaluation

To evaluate the track component, we simulate the track of 555 historical storms during 1979–2014 (initiated from historical locations) in 40 independent runs and compare simulated tracks with observational tracks. We simulate the first two steps of the track using only the local wind, as in the track component in Emanuel et al. (2006). Then the analog model and analog-wind model are applied respectively for the rest of the trajectories until the storm center hits land.

Figure 5 shows the comparison of 60 randomly selected tracks generated by the analog track model and analog-wind track model, with the same initial locations in IBTrACS. We find that although only a slight

JING AND LIN 8 of 18

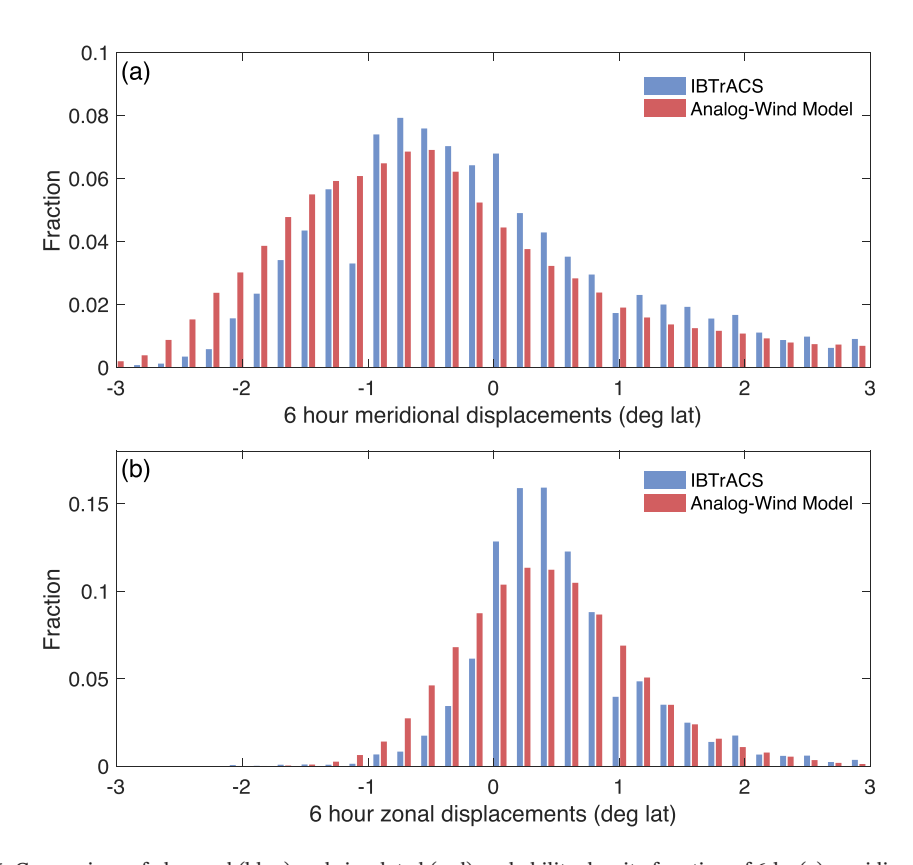


**Figure 6.** Comparison of observed (blue) and simulated (red) probability density function of 6-hr (a) meridional and (b) zonal displacements of storms in 1979–2014. Used for this comparison are 5,550 simulated tracks from 10 independent simulations.

difference appears between the  $\mathbb{R}^2$  values of the models (Table 2), the synthetic tracks from the analog track model are much smoother (with even straight lines) than observations, but this problem is largely resolved in the analog-wind model. In general, the analog-wind model produces more realistic tracks with more tracks executing turnings, meanderings, and crossings. It is noted that the model is relatively robust to initialization; however, it is possible to generate storms that hit South America (where no storm has ever been observed) if the movement in the first two steps is drawn randomly. This observation indicates that the wind-driven initialization is necessary.

A comparison of the 6-hourly meridional and zonal displacements of simulated and observed tracks is shown in Figure 6. The simulation results are largely in good agreement with observations. There exists a slightly positive bias for the negative meridional displacement, a negative bias for the positive meridional displacement, and an overestimation for negative zonal displacements. These biases may induce less recurvation in simulated storm tracks, as can be seen in the comparison of the track density between simulations and observations, shown in Figure 7.

In Figure 7, the colors show the spatial track density normalized by the basin maximum. The simulations capture relatively well the spatial variation of TC tracks in terms of the maxima occurring at the Caribbean Sea, Gulf of Mexico, and U.S. East Coast and near the main development region of TCs. However, the analog-wind model tends to have a negative bias in the magnitude of the local maximum in the Gulf of Mexico. Also, some simulated tracks recurve earlier than historical storms, and the hot spot close to Florida and South Carolina is further off the U.S. coast in the simulation.

#### 3.3. Intensity

In this work, the Markov environment-dependent intensity model, MeHiM, is applied to simulate storm intensity evolution. The development of this model is described in our previous studies, Lin et al. (2017)

JING AND LIN 9 of 18

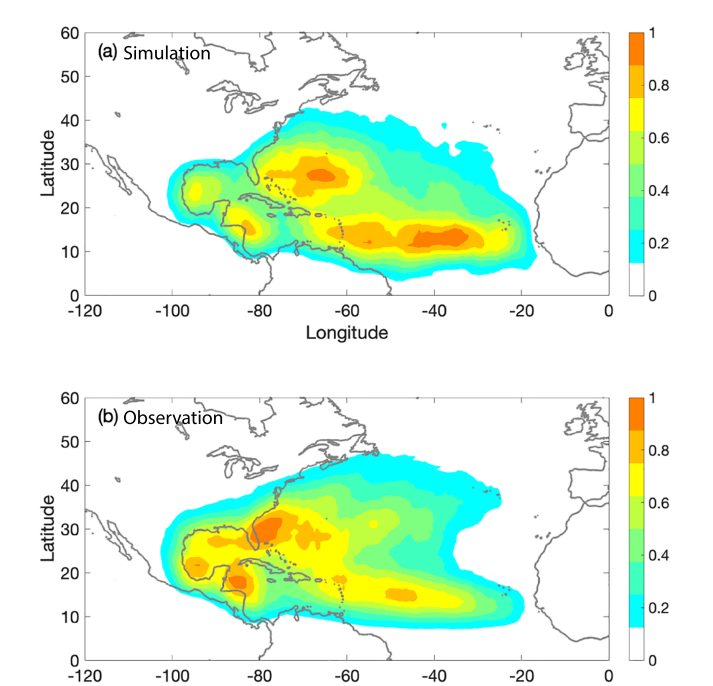


**Figure 7.** Comparison of track density from (a) one simulation with (b) observation in IBTrACS. Track density is calculated as the accumulated number of TC passes into each  $0.75^{\circ} \times 0.75^{\circ}$  grid box normalized by the maximum grid value of the basin, smoothed with a Gaussian low-pass filter. To be consistent with the simulations, the historical tracks are terminated when they hit land.

Longitude

and Jing and Lin (2019), and we refer the reader to these studies for detailed discussions. Here we describe the basic structure and advantages of this model.

The MeHiM is developed to simulate TC intensity evolution dependent on the surrounding large-scale environment. The model considers three unobserved (hidden) discrete states of intensification and associates each state with a probability distribution of intensity change. The three unobserved discrete states, including "static," "moderate," and "extreme" states, represent the storm's slow, normal, and rapid intensity change, respectively. The storm's transit from one state to another is described as a Markov chain. In addition to the storm variables (i.e., V and DV<sub>p</sub>), both the intensity change and state transit components of the model are dependent on environmental variables including PI, SHR, RH, and OCN. In the simulation, the storm's initial state is initialized by a multinomial logistic regression. Then, MeHiM is used to simulate storm intensity evolution when the storm is over the ocean, and a simplified land model (similar to Kaplan & DeMaria, 1995) is added to estimate intensity decay when the storm moves over land. As evaluated extensively by Jing and Lin (2019), the MeHiM improves over previous models including linear and mixture models, as it can better simulate rapid intensification (RI) of storms, which are essential in better capturing the tail of the distribution of the life time maximum intensity (LMI; Lee et al., 2016a, 2016b). The MeHiM provides a "lock-in" mechanism that supports continuous large intensification once the storm enters the extreme state and when the environment is favorable, so that it can simulate a realistic fraction of RI storms, comparable to the observation.

# 4. Integrated TC Model PepC

The three model components are coupled together to form the TC modeling system, PepC. We simulate TCs for the NA basin in the period of 1979–2014 and compare simulated results with historical data to evaluate the performance of PepC. For each year in the simulation, we use the hierarchical Poisson genesis model to estimate the number of storms and location and time of their formation. Then, each storm is propagated by the analog-wind track model. Along the track, the storm's intensity (sustained maximum wind) is initialized by random sampling from the historical data and then simulated with MeHiM, until the storm's intensity becomes lower than 10 kt. To account for the uncertainty in a stochastic modeling system, we conduct 100 realizations of the 36-year simulation (1979–2014). We obtain a total of 55,117 tropical storm seeds, and among the seeds, there are around  $66\% \pm 2\%$  that can intensify and reach TC strength (LMI > 34 kt; 36,311 storms in total). To form a fair comparison with IBTrACS, we remove storms with LMI less than 25 kt, and the remaining 43,979 storms are used for evaluation in the following subsections.

#### 4.1. Genesis Density and ENSO States

After removing tropical storm seeds that cannot grow to 25 kt, the spatial distribution of the remaining genesis (not shown) is similar to that initiated by the genesis component, as shown in Figure 4. This similarity indicates that coupling the track and intensity components with the genesis component do not largely change the spatial distribution of the genesis. A large negative bias still exists in the main development region, which has a significant impact on simulated TC track density in that region, as will be discussed in section 4.2.

As ENSO is a major driver of TC interannual variations, we further examine the phase variability linked to ENSO, especially the shift in genesis location under different ENSO states. Simulations for strong or very strong El Nino years (1982–1983, 1987–1988, 1991–1992, 1997–1998) and La Nina years (1988–1989,1998–2000, 2007–2008, 2010–2011) are compared in Figure 8. In addition to a decrease in the TC rate from El Nino years to La Nina years, different shifts in the genesis location also exist in the two contrasting ENSO phases. As discussed by Elsner et al. (1999), TC genesis tends to move away from the Gulf of Mexico in

JING AND LIN 10 of 18

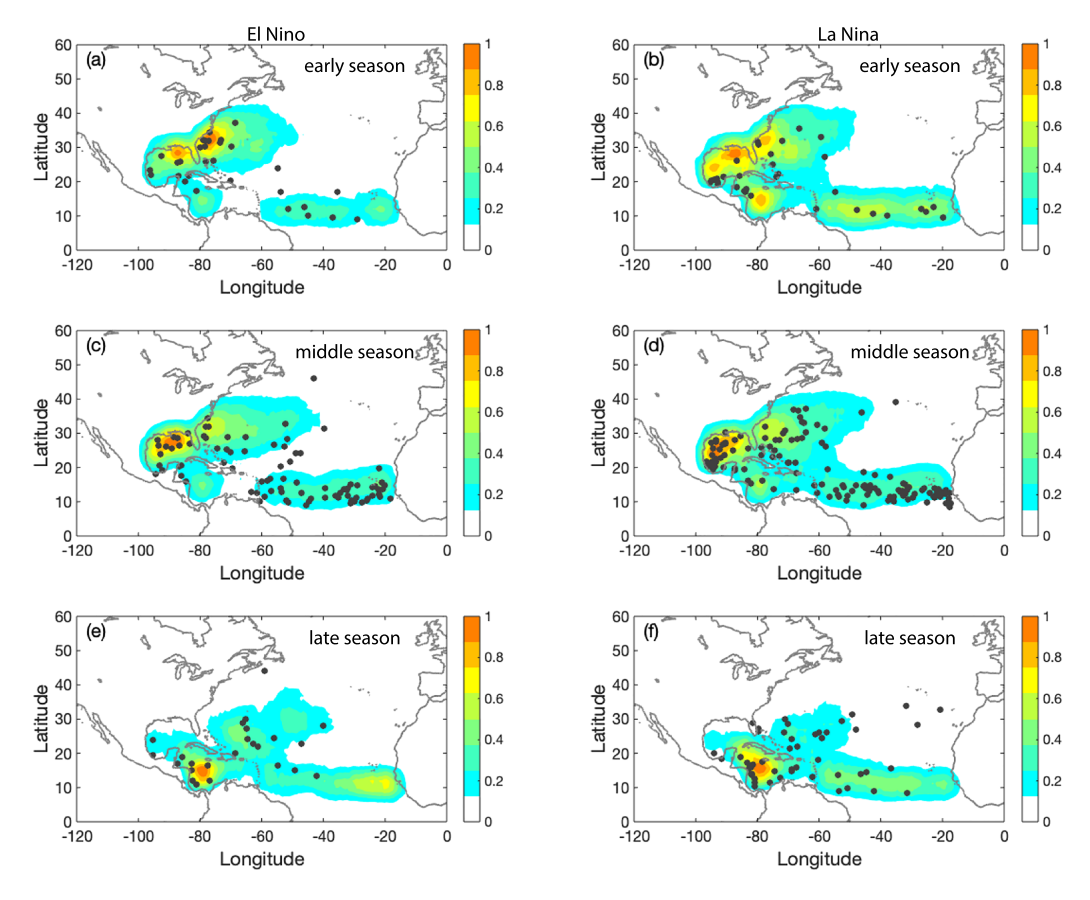


**Figure 8.** Comparison of observed and PepC simulated TC genesis in (a,c,e) El Nino years and (b,d,f) La Nina years. The shifts in simulated and observed genesis locations are compared moving from (a,b) early season (May and June) to (c,d) mid season (July and August) and (e,f) late season (September and October). Black dots represent observed genesis events in 1979–2014. The shades show the simulated genesis density, calculated in the same way as in Figure 4.

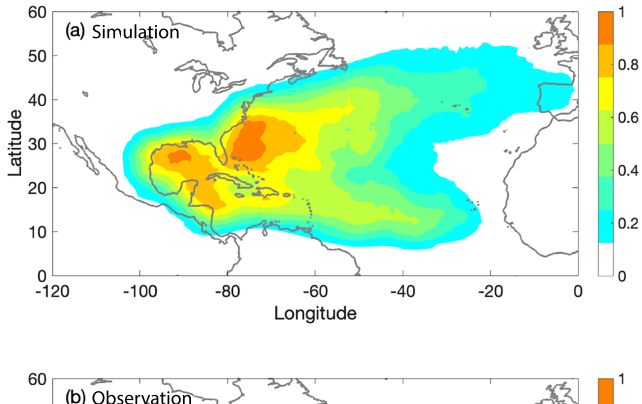
the early season to the Caribbean Sea in the late season during El Nino years. However, in La Nina years, the genesis locations are found off the southeast U.S. coast early in the season, moving toward the Gulf of Mexico in the midseason, and shifting equator-ward over the Caribbean Sea in the late season. On average, TCs tend to form in lower latitudes during La Nina years compared to El Nino years. These historical features are captured by our probabilistic TC model although the model does not directly depend on ENSO indices.

#### 4.2. Track Density and Landfall Frequency

We compare simulated and observed track density in Figure 9. As a land model has been applied to simulate intensity decay over land, we use observed full tracks in this comparison (rather than only the parts over the ocean as shown in Figure 7). Simulations compare relatively well with observations, with the simulated tracks mimicking the typical recurving pattern in observed tracks. However, the area of peak density close to the U.S. coast is larger in the simulation, and the peak density extends farther into the Gulf of Mexico. On the other hand, the large negative bias in the main development region still exist, and it is mostly due to the negative bias in this region of the genesis model.

We further examine regional annual landfall frequency at coastal locations along the NA coastline. To help indicate locations, a total of 186 mileposts (MPs) are defined following Vickery et al. (2000), as shown in Figure 10, to cover the coastline with 100-km spacing along the Mexican coastline and 50-km spacing along the U.S. coastline. As shown in Figure 11, the simulated landfall frequency is in good agreement with observations for almost all mileposts. A slight negative bias exists in the coastal regions near MP 21–31 (lower Gulf of Mexico) and MP 76–91 (west Florida coast), where the observed frequency is near or beyond the upper-75th-percentile bound of the simulated spread. There is also slight positive bias around MP 36–45 (Gulf of Mexico, near the border of United States and Mexico). These biases also appear in the track density

JING AND LIN 11 of 18



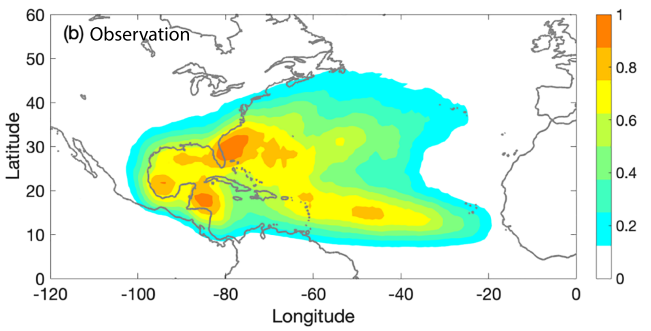


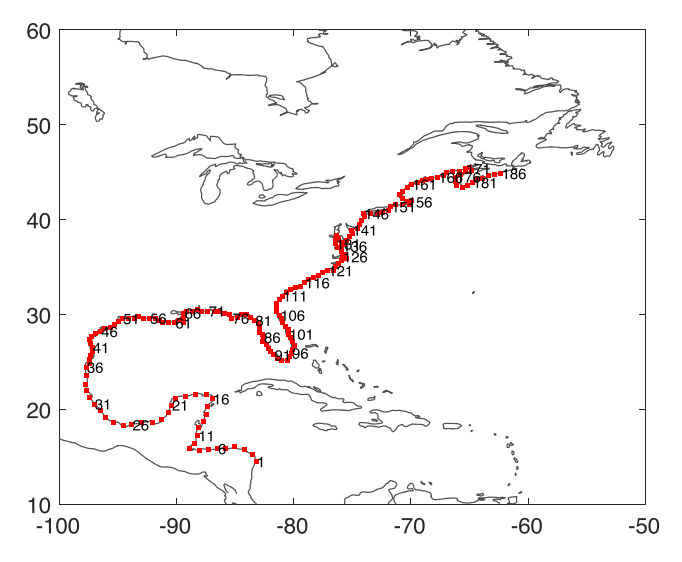
**Figure 9.** Comparison of (a) simulated track density from PepC and (b) observed track density in IBTrACS. Normalized track density is calculated as in Figure 7.

plot in Figure 9. However, even though we see denser tracks in the Caribbean in the observation, the analog-wind model estimates the landfall frequency well for this region (MP 10–13), as landfall is defined as a crossing of the track and coastline segment and many historical tracks passing this region did not hit land. Another interesting result is, though simulated tracks recurve earlier than observations, the landfall frequency is not affected much except for missing the peak around MP 117–120 (near the border of South Carolina and North Carolina), where some historical recurving storms did make landfall. The landfall frequencies for MPs > 125 (Ocean, MA) are in good agreement with observations, except for a slight underestimation near MP 162 and MP 175 (near Portland, ME).

#### 4.3. LMI and Landfall Intensity

Next, we evaluate the intensity of simulated storms. Based on the Saffir-Simpson hurricane wind scale, there are  $14.1 \pm 1.6\%$ ,  $6.4 \pm 1.1\%$ ,  $5.1 \pm 1.0\%$ ,  $3.2 \pm 0.9\%$ , and  $0.9 \pm 0.4\%$  Category 1–5 hurricanes, respectively, in the simulation, compared to 14.1%, 5.6%, 6.3%, 6.1%, and 2.2% in the observation. Our TC model generates a realistic fraction of Cat 1–3 hurricanes, though it underestimates the fraction of Cat 4–5 hurricanes by around 50%. In Figure 12, we further examine the LMI distribution for non-RI and RI storms separately. Among all storms, there are  $21.5\% \pm 1.8\%$  storms undergoing RI in the simulation, which is close to the observation of 24.9% RI storms. Our TC model captures the LMI distribution for both subsets of storms relatively well. A slight shift to larger LMI values exists for non-RI storms in the simu-

lation, which is probably because in MeHiM storms still have a chance to grow and intensify even in moderate environments, while in reality these storms are more likely to stay weak. As for RI storms, the simulated density peak of LMI is about 15 kt underestimated, leading to the underestimation of the most extreme storms, i.e., Cat 4–5 storms. This negative bias in simulating Cat 4–5 hurricanes may come from the limitation of the MeHiM, as discussed in Jing and Lin (2019). It may also come from the bias in genesis and track components. For example, the negative bias of cyclogenesis in the main development region and the positive bias near the coast may result in more TCs with shorter lifespan and less chance for RI toward Cat 4–5 intensities.



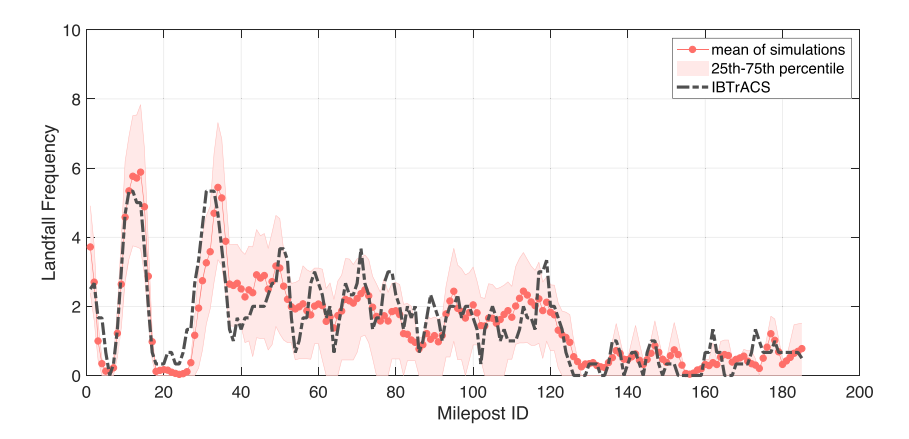
**Figure 10.** Locations of considered mileposts along Mexico (every 100 km) and U.S. (every 50 km) coastline.

Figure 13 shows a comparison of observed and simulated maximum land-fall intensity along the NA coastline. The maximum intensity is defined as the maximum wind speed of all simulated or observed storms that approach within 250 km of each coastal milepost shown in Figure 10. The median of all the 100 simulations is very close to the observations especially in the north of MP 80 (the U.S. coast), and the range of 25th–75th percentiles can mostly cover the observations. The maximum land-fall intensity is underestimated in the Caribbean and the Gulf of Mexico (MP <20), likely due to the fact that the MeHiM has a negative bias in simulating the most extreme storms, which often occur in these regions.

# 4.4. Return Period

To discuss about TC hazard potential on regional scales, we divide the NA coastline into three subregions (North-East United States, South-East United States, and Gulf Coast of Mexico) and calculate the return periods of landfall intensities for the entire NA coastline and for each subregion, as shown in Figure 14. In all four regions, the historic and simulated return period curves compare quite well. As expected, the Gulf of Mexico region has the greatest hazard potential, with the 100-yr landfall intensity greater than 130 kt, in both the observation and simulation.

JING AND LIN 12 of 18



**Figure 11.** Observed (black curve) and simulated (red curve) landfall frequency at each of 186 mileposts (shown in Figure 10) along the NA coastline. The red curve shows the mean and shading represents 25th–75th percentile range based on 100 realizations.

To display the local hazard potential, Figure 15 shows the 100-year return level of the landfall intensity for each of the 186 MPs along the NA coastline. In this plot, all simulated tracks that approach the coastline and are within 250 km of each milepost are used to compute return level for that milepost. The simulation results compare relatively well with observations. The model tends to overestimate the 100-year intensity level along the coastline of Gulf of Mexico, that is, MP 20–100. This positive bias in the return level is induced by an overestimation in simulated track counts in this region. Although the simulation has a similar number of storms crossing the coastline in this region (Figure 11), more simulated tracks pass within 250 km of the mileposts in the region (Figure 9).

## 5. Discussion on Humidity Variables

The TC modeling system is dependent on ambient environmental variables including relative humidity (RH) in both genesis and intensity components. Some of previous studies have suggested using the saturation deficit, rather than RH, to represent the dependence of TC genesis on humidity, for both theoretical and modeling considerations (Emanuel et al., 2008). Saturation deficit (SD) is defined by Emanuel (1995):

$$SD = \frac{s_b - s_m}{s_0^* - s_b},$$
 (2)

where  $s_m$  and  $s_b$  are the entropies of the middle troposphere and boundary layer, respectively, and  $s_0^*$  is the saturation entropy of the sea surface. This thermal parameter regulates the time scale of an initial disturbance to moisten the middle troposphere so that intensification can occur, and thus, it may play an important role in regulating TC genesis and thus storm frequency.

Though the seasonal and spatial variations in  $s_b - s_m$  are dominated by RH under the current climate, this is not the case under global warming (Emanuel et al., 2008). Different choices between RH and SD may even yield conflicting results in simulating TC frequency in a warmer climate. For example, in a recent study, by statistically downscaling six Fifth Coupled Model Intercomparison Project (CMIP5, Taylor et al., 2012) models, Lee et al. (2019) obtained an increasing trend in projected annual mean TC frequency using RH as the humidity predictor and a decreasing trend using SD under Representative Concentration Pathway (RCP) 8.5 scenario. However, by statistical-deterministically downscaling six CMIP5 models for the RCP8.5 scenario, Emanuel (2013) obtained an increasing trend using GPI based on SD.

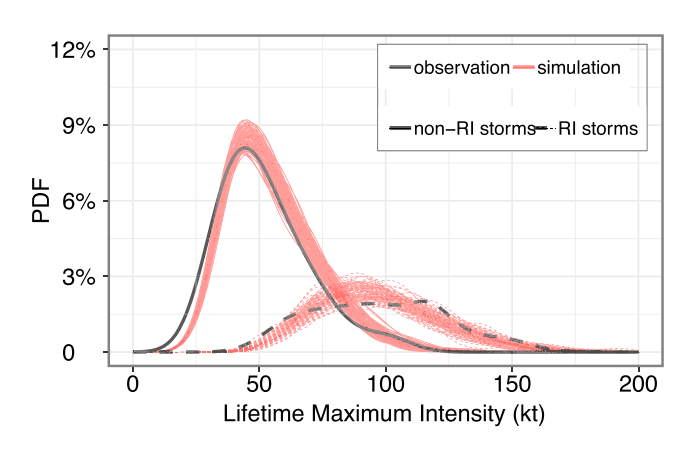


**Figure 12.** Probability density function (PDF) of LMI from historical record (black) and from 100 model simulations (red). Solid and dash lines are PDFs based on subsets of non-RI and RI storms.

JING AND LIN 13 of 18

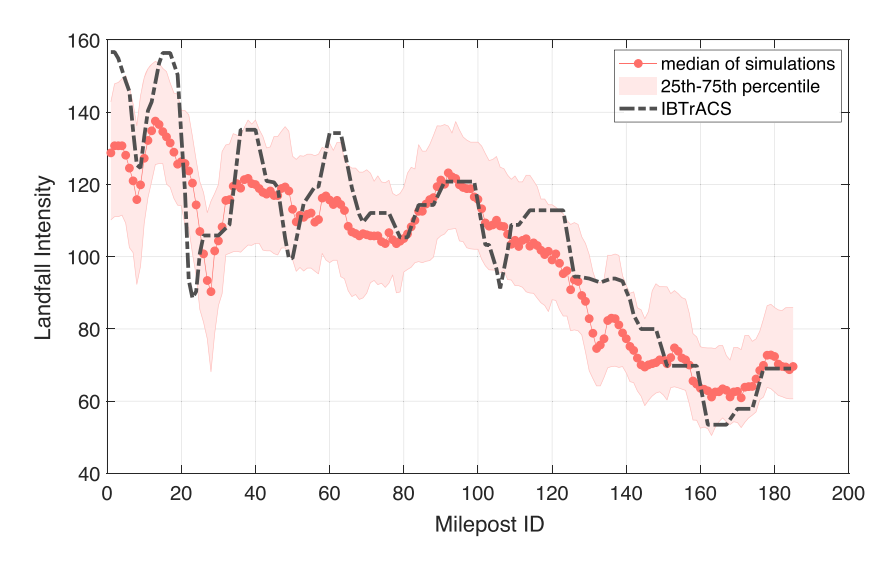


**Figure 13.** Observed (black) and simulated (red) maximum landfall intensity at 186 mileposts (shown in Figure 10) along the NA coastline. The red curve shows the median and shading represents 25th–75th percentile range based on 100 realizations.

To evaluate if SD performs better in TC statistical modeling for the current climate, we develop an alternative TC genesis model using SD in replacement of RH. The simulated annual rates are shown in Figure 16. Simulated TC annual frequency using SD has a correlation of 0.57 with the observation (on testing dataset),

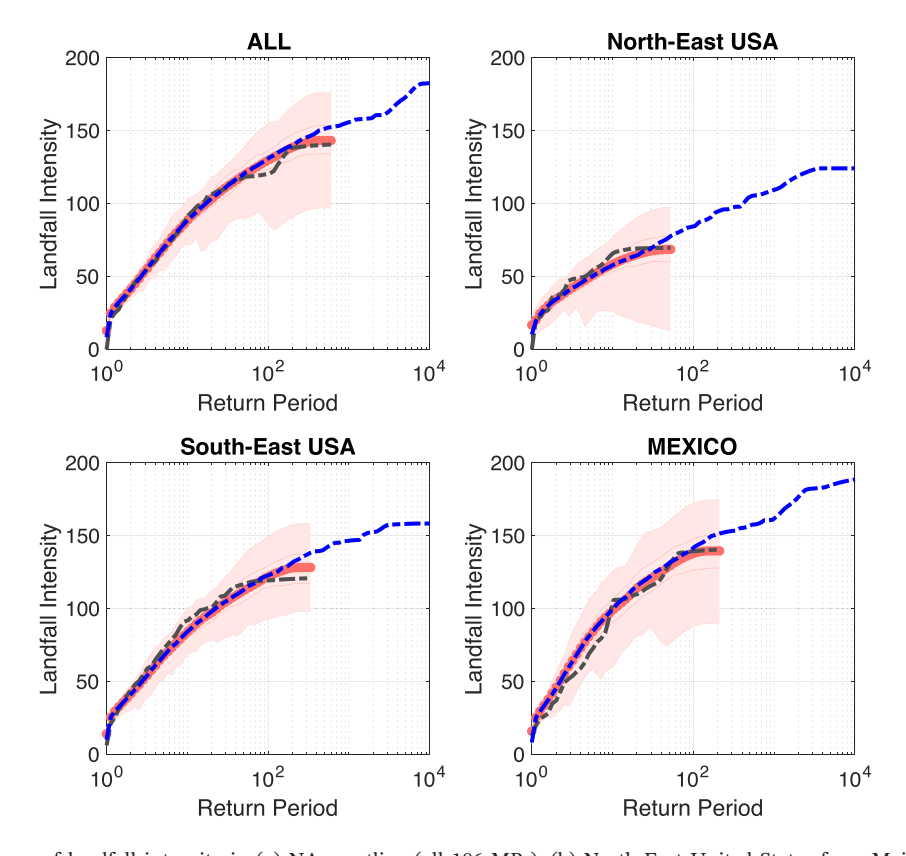


**Figure 14.** Return period curves of landfall intensity in (a) NA coastline (all 186 MPs), (b) North-East United States from Maine to Virginia (MP 128–186), (c) South-East United States from North Carolina to Florida plus Gulf Coast of the United States (MP 41–128), and (d) Gulf Coast of Mexico (MP 1–40). The black dash curves are estimations from the historical record. The red curves show the median and shadings represent 0 to 100 percentiles from 100 simulations over 36 years. The blue dash curves are calculated using all 3,600-year simulations.

JING AND LIN 14 of 18

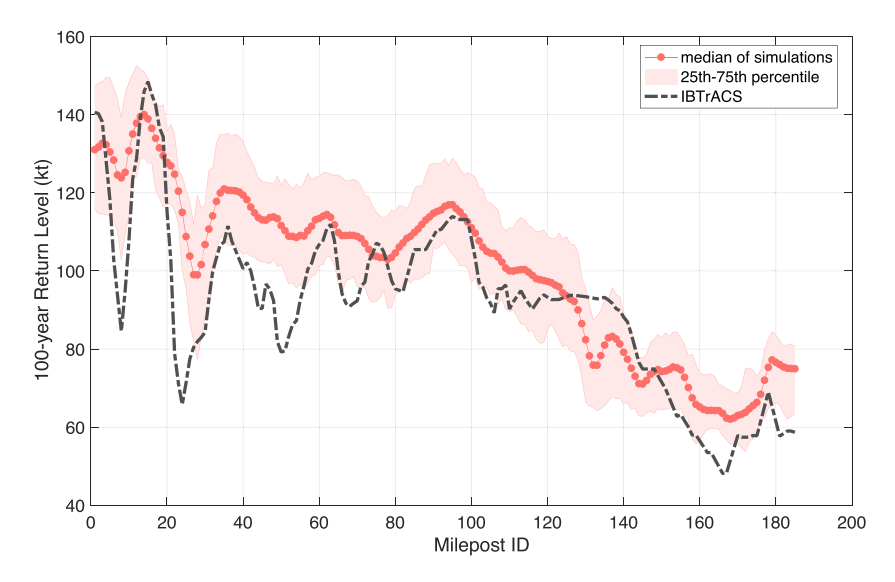


**Figure 15.** Comparison of simulated (red) and observed (black) 100-year landfall intensity at 186 mileposts (shown in Figure 10) along the NA coastline. The red curve shows the median and shading shows the 25th–75th percentile range of 100 simulations.

compared to a correlation of 0.72 using RH. The correlation using RH is significantly higher than that using SD based on Williams' test (Williams, 1959), with a p value less than 0.02. A comparison between Figures 2 and 16 also shows that the model using SD is not as good as the one using RH in simulating the peak values in historical TC frequency. Although SD is preferred over RH for climate change studies given its theoretical basis (Emanuel et al., 2008), in this study, for the current climate simulations, we use RH as it is simpler and renders better simulation results. We suggest further investigation on this matter when applying PepC for future climate simulations.

# 6. Summary

In this work, we have developed an environment-dependent probabilistic TC model, PepC, to simulate synthetic TCs for risk analysis. PepC consists of three model components: a hierarchical Poisson genesis model, an analog-wind track model, and a Markov intensity model, which are integrated to simulate storm's complete lifecycle, from genesis to lysis. The hierarchical Poisson genesis model simulates TC temporal and spatial variations using Poisson regression on clustered grids, where the basin is divided into connected regions such that the environmental conditions are similar within each region. The analog-wind track model is developed based on the BAM assumption in Emanuel et al. (2006) but improved by incorporating storm

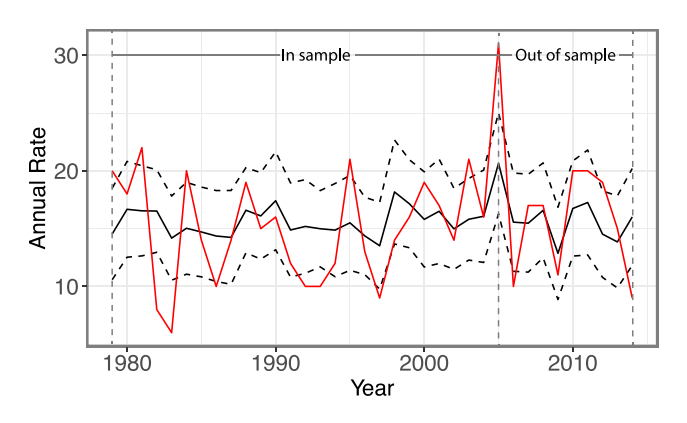


**Figure 16.** Same with Figure 2, but developed based on SD, rather than RH, as the humidity parameter in the genesis model.

analog predictors that represent effects of both storm's inertia and background winds. The intensity model, MeHiM, adopted from Jing and Lin (2019), simulates the storm's intensity evolution using a dependent hidden Markov model, where the storm is assumed to transit among three unobserved states that represent the storm's slow, moderate, and rapid intensity change. The three model components are dependent on local climate variables including absolute vorticity, relative humidity, potential intensity, vertical shear, local winds, and an ocean feedback parameter, which may be taken from either reanalysis data or climate model estimations.

PepC has been evaluated by comparing simulated TC climatology with observations, in the period of 1979–2014 for the NA basin. Simulated TC formations are in good agreement with observations in multiple aspects of climatology statistics including cyclogenesis interannual variation. The differences in TC formation locations under different

JING AND LIN 15 of 18



ENSO phases are also captured. However, there exists a negative bias in simulated TC genesis in the main development region, which leads to a noticeable negative bias in simulated track density near this region. Nevertheless, the bias over this region has relatively little impact on the landfall frequency. Coupled with the hierarchical Poisson genesis model and analog-wind track model, the MeHiM can simulate a similar RI rate as in the observation. While the LMI distribution of simulated storms is in good agreement with observations, including the tail, PepC slightly underestimates the most extreme storms, that is, Cat 4–5 hurricanes. We have further evaluated PepC in terms of estimating regional and local TC hazard potential. The comparison between observations and simulations shows that the model performs well in reproducing landfall frequency, landfall intensity distribution, and return periods of landfall intensities. Therefore, PepC can be used to support TC risk assessment for coastal regions, including those with very limited observational data.

For future work, we plan to further improve the three model components, especially the track component, which partially depends on historical tracks. We also plan to incorporate a size component (Chavas et al., 2016; Chavas & Lin, 2016). The full modeling system will then be coupled with TC hazard models to assess TC-related multihazards, including wind, surge, rainfall, and flooding. Future studies may also include a comparison between the probabilistic TC model and dynamical models, such as the newly developed global climate model, the High-resolution Forecast-Oriented Low Ocean Resolution (HiFLOR; Murakami et al., 2015) of the NOAA Geophysical Fluid Dynamics Laboratory. Ultimately, we will investigate TC hazards and risks in different climates by downscaling the state-of-the-art climate models, such as those from the CMIP5. To do so, we will further investigate the role of RH and SD in regulating TC frequency under the future climate.

#### **DATA AVAILABILITY STATEMENT**

The data used for model development are described in section 2. The hurricane dataset IBTrACS can be accessed from the National Climatic Data Center (https://www.ncdc.noaa.gov/ibtracs/). The atmospheric and oceanic reanalysis data are downloaded from the European Centre for Medium-Range Weather Forecasts (ERA-Interim: https://apps.ecmwf.int/datasets/data/interim-full-daily/levtype=sfc/and Ocean Reanalysis System 4: ftp://ftp-icdc.cen.uni-hamburg.de/EASYInit/ORA-S4/). The generated synthetic storm datasets are deposited to the NSF DesignSafe-CI and can be accessed online (https://www.designsafe-ci.org/data/browser//projects/6938064123887349270-242ac116-0001-012/).

#### Acknowledgments

This study is supported by Grants 1652448 from the National Science Foundation and NA14OAR4320106 from the National Oceanic and Atmospheric Administration, U.S. Department of Commerce. The statements, findings, conclusions, and recommendations herein are those of the authors and do not necessarily reflect the views of the National Science Foundation, the National Oceanic and Atmospheric Administration, or the U.S. Department of Commerce.

# References

- Balmaseda, M. A., Mogensen, K., & Weaver, A. T. (2013). Evaluation of the ECMWF ocean reanalysis system ORAS4. Quarterly Journal of the Royal Meteorological Society, 139, 1132–1161. https://doi.org/10.1002/qj.2063
- Bister, M., & Emanuel, K. (2002). Low frequency variability of tropical cyclone potential intensity 1. Interannual to interdecadal variability. Journal of Geophysical Research, Atmospheres (1984–2012), 107(D24), 4801. https://doi.org/10.1029/2001JD000776
- Bister, M., & Emanuel, K. A. (1998). Dissipative heating and hurricane intensity. Meteorology and Atmospheric Physics, 65, 233–240. https://doi.org/10.1007/BF01030791
- Chavas, D. R., & Lin, N. (2016). A model for the complete radial structure of the tropical cyclone wind field. Part II: Wind field variability. Journal of the Atmospheric Sciences, 73, 3093–3113. https://doi.org/10.1175/JAS-D-15-0185.1
- Chavas, D. R., Lin, N., Dong, W., & Lin, Y. (2016). Observed Tropical Cyclone Size Revisited. https://doi.org/10.1175/JCLI-D-15-0731.1. Dee, D. P., Uppala, S. M., Simmons, A. J., Berrisford, P., Poli, P., Kobayashi, S., et al. (2011). The ERA-interim reanalysis: Configuration and performance of the data assimilation system. *Quarterly Journal of the Royal Meteorological Society*, 137(656), 553–597. https://doi.org/10.1002/qi.828
- Kaplan, J., & DeMaria, M. (1995). A simple empirical model for predicting the decay of tropical cyclone winds after landfall. *Journal of Applied Meteorology*, 34, 2499–2512. https://doi.org/10.1175/1520-0450(1995)034<2499:ASEMFP>2.0.CO;2
- Elsner, J. B., Kara, A. B., & Owens, M. A. (1999). Fluctuations in North Atlantic hurricane frequency. *Journal of Climate*, 12, 427–437. https://doi.org/10.1175/1520-0442(1999)012<0427:FINAHF>2.0.CO;2
- Emanuel, K. (1988). The maximum intensity of hurricanes. *Journal of the Atmospheric Sciences*, 45, 1143–1155. https://doi.org/10.1175/1520-0469(1988)045<1143:TMIOH>2.0.CO;2
- Emanuel, K. (1995). The behavior of a simple hurricane model using a convective scheme based on subcloud-layer entropy equilibrium. Journal of the Atmospheric Sciences, 52, 3960–3968. https://doi.org/10.1175/1520-0469(1995)052<3960:TBOASH>2.0.CO;2
- Emanuel, K. (2010). Tropical cyclone activity downscaled from NOAA-CIRES reanalysis, 1908–1958. *Journal of Advances in Modeling Earth Systems*, 2(1), 1. https://doi.org/10.3894/JAMES.2010.2.1
- Emanuel, K. (2013). Downscaling CMIP5 climate models shows increased tropical cyclone activity over the 21st century. PNAS, 110, 12219–12224. https://doi.org/10.1073/pnas.1301293110
- Emanuel, K. (2017). Assessing the present and future probability of hurricane Harvey's rainfall. PNAS, 114, 12681–12684. https://doi.org/10.1073/pnas.1716222114
- Emanuel, K., DesAutels, C., Holloway, C., & Korty, R. (2004). Environmental control of tropical cyclone intensity. Journal of the Atmospheric Sciences, 61, 843–858. https://doi.org/10.1175/1520-0469(2004)061<0843:ECOTCI>2.0.CO;2

JING AND LIN 16 of 18



- Emanuel, K., & Nolan, D. S. (2004). Tropical cyclone activity and the global climate system. 26th Conference on Hurricanes and Tropical Meteorology, 240–241.
- Emanuel, K., Ravela, S., Vivant, E., & Risi, C. (2006). A statistical deterministic approach to hurricane risk assessment. *Bulletin of the American Meteorological Society*, 87, s1–s5. https://doi.org/10.1175/BAMS-87-3-Emanuel
- Emanuel, K., Sundararajan R., & Williams, J. (2008). Hurricanes and global warming: Results from downscaling IPCC AR4 simulations. Bulletin of the American Meteorological Society, 89, 347–368. https://doi.org/10.1175/BAMS-89-3-347
- Felzenszwalb, P. F., & Huttenlocher, D. P. (2004). Efficient graph-based image segmentation. *International Journal of Computer Vision*, 59, 167–181. https://doi.org/10.1023/B:VISI.0000022288.19776.77
- Gray, W. M. (1975). Tropical cyclone genesis.
- Hall, T. M., & Jewson, S. (2007). Statistical modelling of North Atlantic tropical cyclone tracks. *Tellus A*, 59, 486–498. https://doi.org/10.1111/j.1600-0870.2007.00240.x
- Hall, T. M., & Jewson, S. (2008). Comparison of local and basinwide methods for risk assessment of tropical cyclone landfall. *Journal of Applied Meteorology and Climatology*, 47, 361–367. https://doi.org/10.1175/2007JAMC1720.1
- Hope, J. R., & Neumann, C. J. (1970). An operational technique for relating the movement of existing tropical cyclones to past tracks. Monthly Weather Review, 98(7), 925–933. https://doi.org/10.1175/1520-0493(1970)098<0925:AOTFRT>2.3.CO;2
- Irish, J. L., & Resio, D. T. (2013). Method for estimating future hurricane flood probabilities and associated uncertainty. *Journal of Waterway, Port, Coastal, and Ocean Engineering*, 139, 126–134. https://doi.org/10.1061/(ASCE)WW.1943-5460.0000157
- Jagger, T., Jagger, T., & Niu, X. (2001). A dynamic probability model of hurricane winds in coastal counties of the United States. *Journal of Applied Meteorology*, 40, 853–863. https://doi.org/10.1175/1520-0450(2001)040<0853:ADPMOH>2.0.CO;2
- James, M. K., & Mason, L. B. (2005). Synthetic tropical cyclone database. *Journal of Waterway, Port, Coastal, and Ocean Engineering*, 131, 181–192. https://doi.org/10.1061/(ASCE)0733-950X(2005)131:4(181)
- Jing, R., & Lin, N. (2019). Tropical cyclone intensity evolution modeled as a dependent hidden Markov process. *Journal of Climate*, 32, 7837–7855. https://doi.org/10.1175/JCLI-D-19-0027.1
- Knapp, K. R., Kruk, M. C., Levinson, D. H., Diamond, H. J., & Neumann, C. J. (2010). The international best track archive for climate stewardship (IBTrACS). Bulletin of the American Meteorological Society, 91, 363–376. https://doi.org/10.1175/2009BAMS2755.1
- Lee, C.-Y., Camargo, S. J., & Sobel, A. H., Tippett, M. K. (2019). Statistical-dynamical downscaling projections of tropical cyclone activity in a warming climate: Two diverging genesis scenarios. https://www.ldeo.columbia.edu/~sobel/Papers/Lee\_et\_al\_2019\_CLIM\_submit. pdf
- Lee, C.-Y., Tippett, M. K., Camargo, S. J., & Sobel, A. H. (2015). Probabilistic multiple linear regression modeling for tropical cyclone intensity. *Monthly Weather Review*, 143, 933–954. https://doi.org/10.1175/MWR-D-14-00171.1
- Lee, C.-Y., Tippett, M. K., Sobel, A. H., & Camargo, S. J. (2016a). Autoregressive modeling for tropical cyclone intensity climatology. *Journal of Climate*, 29, 7815–7830. https://doi.org/10.1175/JCLI-D-15-0909.1
- Lee, C.-Y., Tippett, M. K., Sobel, A. H., & Camargo, S. J. (2016b). Rapid intensification and the bimodal distribution of tropical cyclone intensity. *Nature Communications*, 7(1), 1–5. https://doi.org/10.1038/ncomms10625
- Lee, C.-Y., Tippett, M. K., Sobel, A. H., & Camargo, S. J. (2018). An environmentally forced tropical cyclone hazard model. *Journal of Advances in Modeling Earth Systems*, 10, 223–241. https://doi.org/10.1002/2017MS001186
- Lin, N., Emanuel, K., Oppenheimer, M., & Vanmarcke, E. (2012). Physically based assessment of hurricane surge threat under climate change. *Nature Climate Change*, 2, 462–467. https://doi.org/10.1038/nclimate1389
- Lin, N., Jing, R., Wang, Y., Yonekura, E., Fan, J., & Xue, L. (2017). A statistical investigation of the dependence of tropical cyclone intensity change on the surrounding environment. *Monthly Weather Review*, 145, 2813–2831. https://doi.org/10.1175/MWR-D-16-0368.1
- Marks, D. G. (1992). The beta and advection model for hurricane track forecasting (NOAA Tech. Memo. NWS NMC 70, 89 Pp.). Camp Springs, MD: National Meteorological Center.
- Marsooli, R., Lin, N., Emanuel, K., & Feng, K. (2019). Climate change exacerbates hurricane flood hazards along US Atlantic and gulf coasts in spatially varying patterns. *Nature Communications*, 10(1), 1–9. https://doi.org/10.1038/s41467-019-11755-z
- Mendelsohn, R., Emanuel, K., Chonabayashi, S., & Bakkensen, L. (2012). The impact of climate change on global tropical cyclone damage. Nature Climate Change, 2(3), 205–209. https://doi.org/10.1038/nclimate1357
- Menkes, C. E., Lengaigne, M., Marchesiello, P., Jourdain, N. C., Vincent, E. M., Lefèvre, J., et al. (2011). Comparison of tropical cyclogenesis indices on seasonal to interannual timescales. *Climate Dynamics*, 38, 301–321. https://doi.org/10.1007/s00382-011-1126-x
- Mumane, R. J., Barton, C., Collins, E., Donnelly, J., Eisner, J., Emanuel, K., et al. (2000). Model estimates hurricane wind speed probabilities. Eos, Transactions American Geophysical Union, 81, 433–438. https://doi.org/10.1029/00EO00319
- Murakami, H., Vecchi, G. A., Underwood, S., Delworth, T. L., Wittenberg, A. T., Anderson, W. G., et al. (2015). Simulation and prediction of category 4 and 5 hurricanes in the high-resolution GFDL HiFLOR coupled climate model\*. *Journal of Climate*, 28, 9058–9079. https://doi.org/10.1175/JCLI-D-15-0216.1
- Rumpf, J., Weindl, H., Höppe, P., Rauch, E., & Schmidt, V. (2007). Stochastic modelling of tropical cyclone tracks. Mathematical Methods of Operational Research, 66(3), 475–490. https://doi.org/10.1007/s00186-007-0168-7
- Rumpf, J., Weindl, H., Höppe, P., Rauch, E., & Schmidt, V. (2009). Tropical cyclone hazard assessment using model-based track simulation. Natural Hazards, 48(3), 383–398. https://doi.org/10.1007/s11069-008-9268-9
- Schade, L. R., & Emanuel, K. (1999). The ocean's effect on the intensity of tropical cyclones: Results from a simple coupled atmosphereocean model. *Journal of the Atmospheric Sciences*, 56, 642–651. https://doi.org/10.1175/1520-0469(1999)056<0642:TOSEOT>2.0.CO;2
- Schenkel, B. A. (2016). A climatology of multiple tropical cyclone events. *Journal of Climate*, 29(13), 4861–4883. https://doi.org/10.1175/ JCLI-D-15-0048.1
- Smith, A. B., & Matthews, J. L. (2015). Quantifying uncertainty and variable sensitivity within the US billion-dollar weather and climate disaster cost estimates. Natural Hazards, 77, 1829–1851. https://doi.org/10.1007/s11069-015-1678-x
- Taylor, K. E., Stouffer, R. J., & Meehl, G. A. (2012). An overview of CMIP5 and the experiment design. Bulletin of the American Meteorological Society, 93(4), 485–498. https://doi.org/10.1175/BAMS-D-11-00094.1
- Tippett, M. K., Camargo, S. J., & Sobel, A. H. (2011). A Poisson regression index for tropical cyclone genesis and the role of large-scale vorticity in genesis. *Journal of Climate*, 24, 2335–2357. https://doi.org/10.1175/2010JCLI3811.1
- Tolwinski-Ward, S. E. (2015). Uncertainty quantification for a climatology of the frequency and spatial distribution of North Atlantic tropical cyclone landfalls. *Journal of Advances in Modeling Earth Systems*, 7, 305–319. http://doi.org/10.1002/2014MS000407
- Vickery, P. J., Masters, F. J., Powell, M. D., & Wadhera, D. (2009). Hurricane hazard modeling: The past, present, and future. *Journal of Wind Engineering and Industrial Aerodynamics*, 97, 392–405. https://doi.org/10.1016/j.jweia.2009.05.005

JING AND LIN 17 of 18



# **Journal of Advances in Modeling Earth Systems**

10.1029/2019MS001975

- Vickery, P. J., Skerlj, P. F., & Twisdale, L. A. (2000). Simulation of hurricane risk in the U.S. using empirical track model. *Journal of Structural Engineering*, 126(10), 1222–1237. https://doi.org/10.1061/(ASCE)0733-9445(2000)126:10(1222)
  Williams, E. J. (1959). *Regression analysis*, (Vol. 1959). New York: Wiley.
- Yeo, D. H., Lin, N., & Simiu, E. (2014). Estimation of hurricane wind speed probabilities: Application to New York City and other coastal locations. *Journal of Structural Engineering*, 140(6), 04014017. https://doi.org/10.1061/(ASCE)ST.1943-541X.0000892
- Yonekura, E., & Hall, T. M. (2011). A statistical model of tropical cyclone tracks in the Western North Pacific with ENSO-dependent cyclogenesis. *Journal of Applied Meteorology and Climatology*, 50, 1725–1739. https://doi.org/10.1175/2011JAMC2617.1
- Yonekura, E., & Hall, T. M. (2014). ENSO effect on east Asian tropical cyclone landfall via changes in tracks and genesis in a statistical model. *Journal of Applied Meteorology and Climatology*, 53, 406–420. https://doi.org/10.1175/JAMC-D-12-0240.1

JING AND LIN 18 of 18